



Compare Analysis for the Nanotoxicity Effects of Different Amounts of Endocytic Iron Oxide Nanoparticles at Single Cell Level

Chen-Yu Huang¹, Tzong-Rong Ger², Zung-Hang Wei^{1*}, Mei-Feng Lai^{2*}

¹ Department of Power Mechanical Engineering, National Tsing Hua University, Hsinchu, Taiwan, ² Institute of NanoEngineering and MicroSystems, National Tsing Hua University, Hsinchu, Taiwan

Abstract

Developing methods that evaluate the cellular uptake of magnetic nanoparticles (MNPs) and nanotoxicity effects at single-cellular level are needed. In this study, magnetophoresis combining fluorescence based cytotoxicity assay was proposed to assess the viability and the single-cellular MNPs uptake simultaneously. Malignant cells (SKHep-1, HepG2, HeLa) were incubated with 10 nm anionic iron oxide nanoparticles. Prussian blue stain was performed to visualize the distribution of magnetic nanoparticles. MTT and fluorescence based assay analyzed the cytotoxicity effects of the bulk cell population and single cell, respectively. DAPI/PI stained was applied to evaluate death mechanism. The number of intracellular MNPs was found to be strongly correlated with the cell death. Significant differences between cellular MNP uptake in living and dead cells were observed. The method could be useful for future study of the nanotoxicity induced by MNPs.

Citation: Huang C-Y, Ger T-R, Wei Z-H, Lai M-F (2014) Compare Analysis for the Nanotoxicity Effects of Different Amounts of Endocytic Iron Oxide Nanoparticles at Single Cell Level. PLoS ONE 9(5): e96550. doi:10.1371/journal.pone.0096550

Editor: Bing Xu, Brandeis University, United States of America

Received: January 14, 2014; **Accepted:** April 8, 2014; **Published:** May 13, 2014

Copyright: © 2014 Huang et al. This is an open-access article distributed under the terms of the Creative Commons Attribution License, which permits unrestricted use, distribution, and reproduction in any medium, provided the original author and source are credited.

Funding: This work was supported partly by the ROC National Science Council Grant Numbers NSC 99-2112-M-007-016-MY3, NSC 99-2112-M-007-015-MY3, NSC 102-2112-M-007-006-MY3 and NSC 102-2112-M-007-012 -MY3. No additional funding sources for this study. The funders had no role in study design, data collection and analysis, decision to publish, or preparation of the manuscript.

Competing Interests: The authors have declared that no competing interests exist.

* E-mail: wei@pme.nthu.edu.tw (ZHW); mflai@mx.nthu.edu.tw (MFL)

Introduction

Nanoparticles (NPs) have raised a broad interest in the field of material science or medicine [1], [2], [3], [4]. Due to the larger surface area of NPs which increase the interactions between NPs and cell membrane, the internalization of NPs by cells is effective and which is attractive for delivering drugs, probes or proteins [5], [6], [7]. Among the NPs, magnetic iron oxide NPs are considered highly biocompatible and commonly used for biomedical applications as magnetic resonance imaging (MRI) contrast agents [8], [9], to magnetically label the cells for cell separation [10] and cell sorting [11] or as heat generators for magnetic hyperthermia (MH) [12], [13].

However, cells must be labeled with large amounts of magnetic NPs (MNPs) in order to be manipulated by the above techniques, but may suffer from nanotoxicity. The main process involved in MNPs internalization is endocytosis [14], which is subjected to cell-to-cell variations [15]; therefore, nanotoxicity effects induced by MNPs should be analyzed more accurately on individual cells instead of masking by the average value of bulk measurements. Consequently, methods that assess the cellular uptake of MNPs and nanotoxicity effects at single-cell level are more reasonable than those for bulk-cell assays. Unfortunately, most of the current methods evaluate the internalized iron oxide MNP from a population of cells rather than a single cell. In addition, those techniques including Prussian blue staining [16], T2 relaxometry [17], UV/VIS spectrometry [18], [19], and atomic absorption spectroscopy (AAS) [20], [21] analyze the cells that are non-viable. Until 2002, Wilhelm *et al.* proposed magnetophoresis as a method

to quantify the amounts of internalized MNPs [22]. Later in 2008, Jing *et al.* showed that magnetophoresis could not only analyze cells that remain active but also reveal the differences of uptake capacities between individual cells [23].

In regards to nanotoxicity, not only the exposure concentration/dosage but also the intrinsic properties of the nanoparticles such as surface coating or particle size, were found to be correlated with the induced nanotoxicity [24]. Studies have also observed the changes of cell morphology [25] or cytoskeleton and the increase of reactive oxygen species (ROS) [26] in response to the overloading of iron oxide NPs. From results given by Soenen *et al.*, the cytoskeleton defects have shown to be dependent on the intracellular MNP concentrations [27], [28]. The above studies about nanotoxicity, however, determined the concentration of MNPs in a statistical/bulk manner instead of single cell level; that is, nanotoxicity influenced by MNP number in an individual cell has yet to be studied. Besides, cell-to-cell distinction on MNPs uptake remains unclear. Assays based on flow-cytometry have been considered a standard method to determine the overall cell functioning of individual cell. Unfortunately, the flow-cytometry that combined the function of fluorescence analysis and quantification of MNPs has not readily been available. In this study, a simple strategy is proposed to utilize single cell magnetophoresis with fluorescence based cytotoxicity assay to examine the number of internalized MNPs and the corresponding cell viability simultaneously.

Methods

Cell culture and incubation with magnetic nanoparticles

Three cell lines, SKHep-1 (human liver adenocarcinoma) [29], HepG2 (hepatocellular carcinoma) [30] and HeLa (cervical adenocarcinoma) [31] were maintained in high-glucose Dulbecco's modified Eagle's medium (DMEM) supplemented with 10% fetal bovine serum, 100 U/mL penicillin and 100 mg/mL streptomycin (Gibco). The cells were cultured at 37°C in 5% CO₂ and passaged regularly to maintain exponential growth. After seeded in 6-well culture plates to reach 80–90% confluence, the cells were changed to medium containing 10 nm anionic MNPs (iron concentration in cell medium of 260 µg/mL) (Ferrotec Corp., EMG 705) and subsequently incubated for different time periods (8, 12, 24 h). The anionic MNPs chosen in this study possess negative surface charges which is suitable for either phagocytic or non-phagocytic cell [32], [33].

Prussian blue staining

To verify the intracellular localizations of MNPs, the cells treated with MNPs were washed with phosphate-buffered saline (PBS) for three times and fixed in 4% paraformaldehyde. Thereafter, Prussian blue stain reagent (2% potassium ferrocyanide with 6% HCl (1:1 v/v)) were added to the cells and incubated for 10 min. Finally, cells were counterstained by nuclear fast red to visualize the cell nuclei.

Quantification of cellular uptake of MNPs by magnetophoresis

The experimental procedure and setups for single cell magnetophoresis were similar to that was previously described [34]. Initially, a permanent magnet was adapted to the apparatus of an inverted fluorescence microscope (Olympus CKX41) which was equipped with blue, green & UV filters. The magnetic field was calibrated and the uniformity of the magnetic field was assured before conducting magnetophoresis. The magnetic cells suspended in DMEM medium were submitted to the magnetic field. In the steady state regime, the magnetic force $F_m = m_{bead} dB/dx$ (m_{bead} is the magnetic moment of the magnetic beads and dB/dx is the magnetic field gradient) was balanced with the viscous force $F_{vis} = 6\pi\eta Rv$ (R is the radius of cell, η is the viscosity of the carrier

liquid, v is the cell velocity). The total magnetic moment of the MNPs inside a cell could be expressed as $m_{bead} = NcM_s\pi D^3/6$, where N is the total number of MNPs per cell, D is the diameter of a magnetic nanoparticle, and c is the ratio of the net magnetization

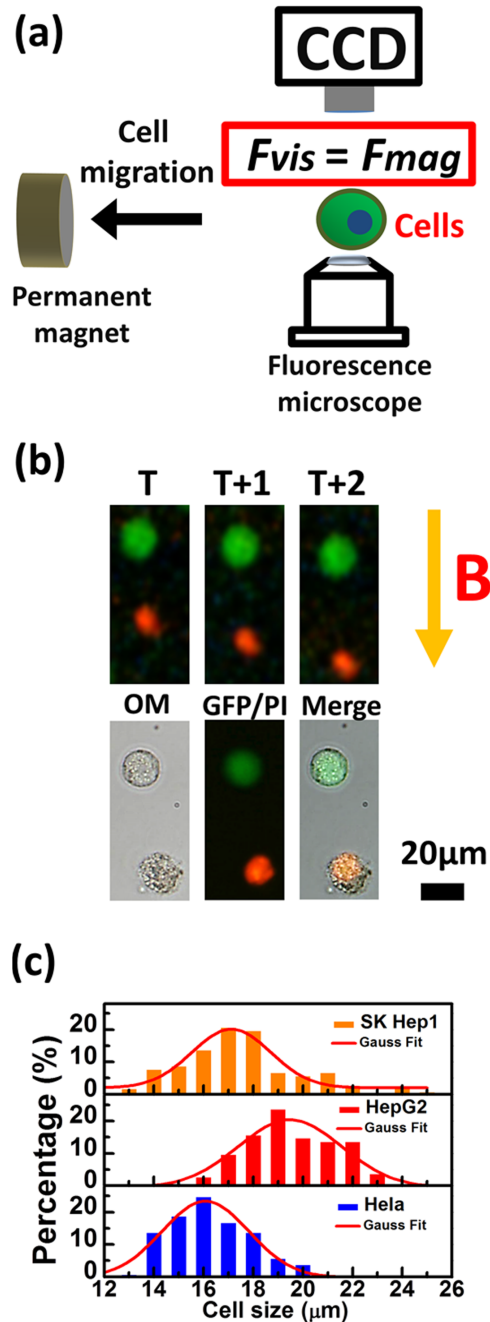


Figure 2. Magnetophoresis and living cell imaging. (a) Schematic representation of cell magnetophoresis. F_{mag} and F_{vis} indicate the magnetic force and the viscous force. (b) (Top) Consecutive magnetophoresis images of two cells move at constant speed (Bottom) Fluorescence image, optical microscope image and the merged image of the two cells. Green, live cells expressed green fluorescent protein (GFP); Red, nucleic acid stained by propidium iodide (PI). The scale bar represents 20 µm. (c) Size distributions of distinctive cells (SKHep-1, HepG2 and HeLa). The red lines are the standard normal distribution. N = 200 cells. doi:10.1371/journal.pone.0096550.g002

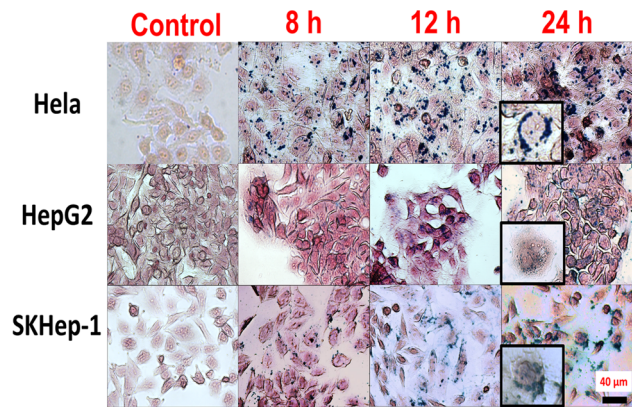


Figure 1. Prussian blue staining results of cancer cells internalizing magnetic nanoparticles (MNP) in a time dependent manner. Control corresponds to the cells (HepG2, SKHep-1, HeLa) that were not treated with MNPs and maintained for 24 h in parallel to the treated groups. Insets: the enlarged images of cells. Blue: MNPs; Red: nucleus. The scale bar in each image represents 40 µm. doi:10.1371/journal.pone.0096550.g001

of MNPs to their saturation magnetization M_s . As the applied magnetic field was 115 mT, the magnetization corresponded to 80% of the magnetization at saturation ($M_s = 484$ kA/m), and thus c could be set to 0.8. By setting the radiuses R of cells and the viscosity of the carrier liquid η as 0.013 Pas, the number of MNPs loaded by cells N could be calculated by the following equation:

$$N = \frac{36\eta Rv}{cM_s D^3 dB/dX} \quad (1)$$

Image analysis and equipment

The mobile cells that were attracted by the magnetic force and moved with constant speed were recorded by a high resolution cooled colored CCD camera (Micro-shot Technology Mshot). The cells were tracked for 15–20 min at one frame per second, and the image sequences were then imported into the public domain open source software, ImageJ (<http://rsb.info.nih.gov/ij/>, NIH, Bethesda, MD), and the displacements of individual cells were tracked via the plug-in “manual tracking” (<http://rsb.info.nih.gov/ij/plugins/track/track.html>, developed by F. Cordelières). To determine the cell radius, the images of cells from optical microscope was captured by CCD camera and analyzed through the built-in measurement tool of the capture software (Mshot Digital Imaging System).

Analysis of cytotoxic effects of bulk cell population by MTT

Cells incubated with MNPs were performed MTT assay to analyze the cytotoxicity effects of bulk cell population. The reagent stock was prepared by dissolving MTT (3-(4, 5-dimethylthiazol-2-yl)-2, 5-diphenyl tetrazolium bromide), (Alfa Chemical Corp.) in PBS to reach a concentration of 5 mg/mL. Later, the stock solution was added to the cell medium in a 1:9 (v/v) volume ratio and the cells were incubated back into the incubator for another 4 h. The supernatant in each well was then removed carefully, changed to 100% Dimethyl sulfoxide (DMSO) solution. After 10 min of mild shaking, the formazan product would be dissolved by DMSO and the absorbance ($\lambda = 570$ nm) was measured by a microplate reader. Cell viability was expressed as the percentage of the absorption of cells treated with MNPs in comparison with that of control cells.

Single-cellular fluorescence imaging distinguishing living, apoptotic or necrotic cell

In order to visualize fluorescent signal produced by live cell, all cells were transfected with green fluorescent protein (GFP) gene [35]. Thereafter, cells were adjusted to a concentration of 10^6 cells/100 μ L PBS. For PI staining [36], 5 μ L of propidium iodide (PI) (stock = 10 μ g/mL, Invitrogen) was mixed with the cell solution and incubated in the dark for 15 min. For DAPI staining, 1 μ L of 4, 6-Diamidino-2-phenylindole dihydrochloride (2 μ g/mL) (Sangon Biotech) was added and cells were incubated in the dark for 10 mins, washed and resuspended by medium sequentially. To define the percentage of normal, apoptotic and necrotic cell, 400 nuclei were counted in random microscopic field. The cell viability from single-cellular analysis was calculated by analyzing the fluorescence images randomly gathered from each group, and the ratio of survival to total cell number was regarded as viability (PI-positive cells with cell necrotic or late apoptotic nuclei). Right before magnetophoresis, we stained GFP-expressed cells with PI to track and analyze the fluorescence emission and the

movement of each cell individually such that the information of viability and velocity for individual cell can be obtained simultaneously.

Statistical analysis

Statistical analysis was performed using Origin 8 Pro (OriginLab Corporation, Northampton, MA). The values acquired from a population of cells were represented as mean \pm standard deviation (SD). At least three independent tests were performed to reach the final results. Linear regression determined the correlation between the mean MNP number obtained from magnetophoresis and the viability of the cells. Student's t-test was used to compare the MNP uptake between the live and dead cells in distinct cell types, and the degree of significance was given as * $p < 0.05$; ** $p < 0.01$; *** $p < 0.001$.

Results and Discussion

The cellular uptake of MNPs was evaluated by Prussian blue stain, as shown Fig. 1. Several intracellular blue-stained vesicles appeared in the cytoplasm of HepG2, HeLa and SKHep-1. Large and dense blue-stained vesicles showed as the incubation period increased, which suggested the time-dependent uptake of the anionic MNPs. In contrast, no blue deposits appeared in cells that were not treated with MNPs and maintained in parallel to the treated group (control). In Fig.2 a, the magnetic force, $F_m = m_{bead} dB/dx$ that exerted on the cells possessing magnetic moment, was balanced with the viscous force, $F_{vis} = 6\pi\eta Rv$ that resisted the movement of the cells caused by the motion of the cell in the medium. Therefore, the related number of intracellular MNPs could be measured as cell moved at constant speed. Fig. 2b shows the sequential micrographs of the cells whose viability was

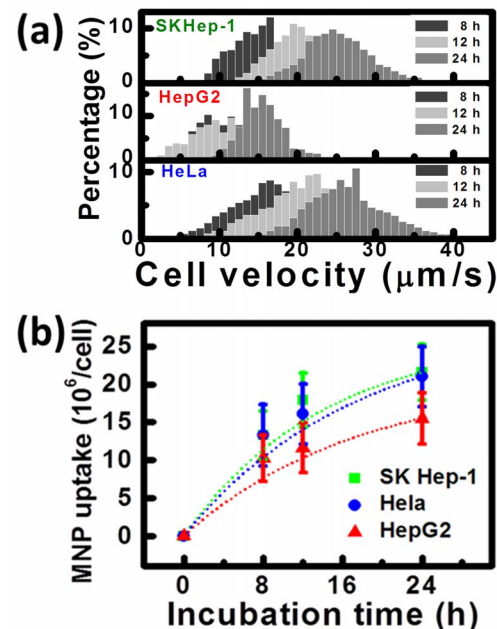


Figure 3. Quantitative analysis of magnetic nanoparticle (MNP) monitored as a function of the incubation time. (a) The distributions of magnetophoretic velocity of cells incubated with magnetic nanoparticles for 8, 12, 24 h. $N = 1000$. (b) The cell loading with MNPs after incubating for 8, 12 and 24 h. Dot lines represent the exponential fit of the data. Bars represent the standard deviation of 500 different cells. doi:10.1371/journal.pone.0096550.g003

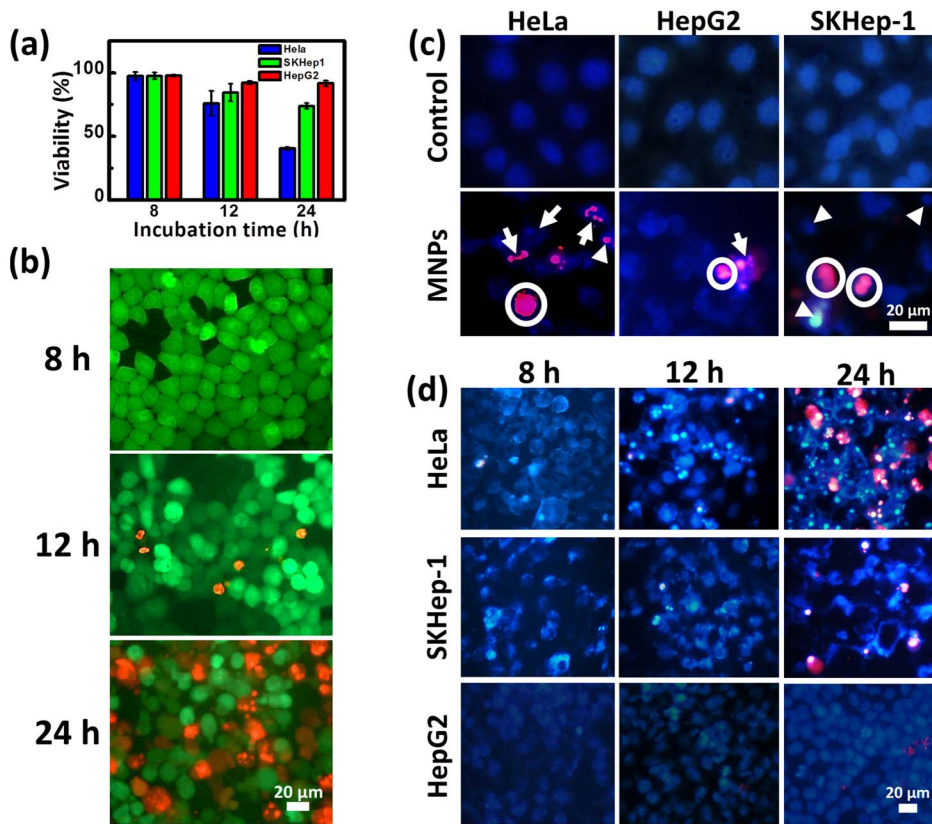


Figure 4. Cytotoxicity effects of single cell and bulk cell populations. (a) Cytotoxicity effects were analyzed by MTT. The data represents as the mean \pm SD, and acquired from 3 independent tests. (b) The cytotoxicity effects of HeLa cells are shown by the overlay fluorescence images of GFP and PI as the MNP incubation time increased from 8 to 24 h. Green, live cells expressed green fluorescent protein (GFP); Red, dead cells stained by PI. The scale bar represents 40 μ m. (c) Overlay fluorescence images of DAPI/PI stain distinguishing mechanisms of cell death (SKHeP-1, HepG2 and HeLa) after treating with MNPs for 24 h. Control: cells were not treated with MNPs for 24 h in parallel to the treated groups. Apoptotic nuclei stained with DAPI showed intense blue fluorescence corresponding to chromatin condensation (indicated by arrow heads) and fragmentation (indicated by arrows). Defective cell membrane allowed PI to enter cytoplasm indicating that cells underwent late apoptosis or necrosis. Possible necrotic cell that correspond to those without clear nuclear fragment but stained with intense PI were circled. (d) Time course experiment of the DAPI/PI staining for the three kinds of cells.

doi:10.1371/journal.pone.0096550.g004

evaluated by the fluorescence probe. Since the viscous force is directly proportional to the radius of cell R , optical micrographs were obtained to analyze the cell radius (shown in Fig. 2c). The mean radiuses for HepG2, SKHeP-1, and HeLa cells are 10 μ m, 8.5 μ m and 7.9 μ m, respectively.

From Fig. 3a, the magnetophoretic velocities from different cells showed Gaussian distributions which were enlarged and right shifted with the increase of time. Based on (1), the amounts of MNPs were counted from the corresponding velocity of the mobile cell and the data were plotted with the exponential fit, as shown in Fig. 3b. For SKHeP-1 cells, the numbers of MNPs increased from (15.53 ± 3.1) to $(21.59 \pm 3.69) \times 10^6$ /cell, whereas for HeLa cells, the number increased from (13.36 ± 4.01) to $(21.01 \pm 3.98) \times 10^6$ /cell. Only a slightly increased for MNP uptake of HepG2 cells, which was from (11.17 ± 3.35) to $(15.3 \pm 3.02) \times 10^6$ /cell. Interestingly, though SKHeP-1 and HepG2 were both derived from liver, SKHeP-1 uptake MNPs more effectively. According to previous research, SKHeP-1 could be regarded as liver sinusoidal endothelial cells (LSEC); therefore, the better cellular uptake efficiency could be contributed to their remarkable endocytic activities [37].

Cytotoxicity effects were analyzed by bulk cell measurement, MTT as well as single-cellular fluorescence based assay. In Fig. 4a,

over 90% of cell remained viable for HepG2 after 24 h of incubated with MNPs; whereas for HeLa and SKHeP-1 cell, the viability decreased from 78% to 40% and 97% to 73%, respectively. MTT assay was based on the reduction of tetrazolium dye by NAD(P)H-dependent oxidoreductase enzymes in the cytosolic compartment of the cell [38]. The decrease of cell viability may be caused by the interaction between MNPs and the subcellular membrane molecule and affected metabolism [24], [39]. Researches have suggested that cells exposed to iron oxide NPs may undergo apoptosis [40]; therefore, DAPI/PI stained was applied to evaluate death mechanism. Apoptotic cells was characterized by abnormal, condensed or fragment chromosome stained by DAPI dye; while for PI dye, it penetrated dead cell membranes to bind to the intracellular DNA, and identified both late-apoptotic and necrotic cells as non-viable cells. In Fig. 4b, the number of non-viable HeLa cells stained by PI increased with the incubation time, which was similar to the result obtained from MTT. In Fig. 4c, the DAPI/PI staining indicated that cells underwent late apoptosis or necrosis after treating with MNPs for 24 h. As high as 61% cells were in necrosis/late-apoptosis for HeLa, as illustrated in Table 1. To prove that cells were traversing through early apoptosis before reaching late apoptosis/necrosis, time course experiment was performed (shown in Fig. 4d). After

Table 1. The mean percentage of normal, apoptotic and necrotic cell stained with DAPI/PI.

Cell	% Normal*			% Apoptosis [†]			% Late apoptosis/necrotic [‡]		
	8 h	12 h	24 h	8 h	12 h	24 h	8 h	12 h	24 h
HeLa	87.91±2.94	34.5±3.04	19±5.03	10.25±2.87	43±2.25	20±1.5	1.84±0.87	22.5±0.8	61±3.6
SKHep-1	87.63±1.4	63.5±3.22	65.8±3	10.75±1.7	22±3.1	9.6±1.15	1.61±0.33	14.5±0.92	24.6±5.13
HepG2	96.09±0.88	93±2	90.1±1.1	3.51±0.85	1±0.5	2.8±0.4	0.4±0.1	6±2	7.1±1.15

*With homogenous DAPI.

[†]Condensed or fragmented DNA stained by DAPI.

[‡]Defective cell membrane stained by PI.

doi:10.1371/journal.pone.0096550.t001

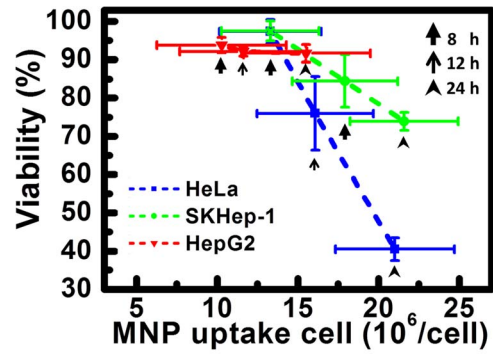


Figure 5. The correlation between the number of internalized MNPs and cell viability. The three data points for each cell type represent the three incubation times (8, 12, 24 h) with MNPs. The ratio of survival to total cell number was regarded as viability (PI-positive cells with cell necrosis or late apoptotic nuclei were regarded as dead cells). The error bars represent the standard deviations (SD) obtained from three independent replicates. The correlation between the mean MNPs number obtained from magnetophoresis and the viability of the cells was determined by linear regression.
doi:10.1371/journal.pone.0096550.g005

the initially 8 h of incubation time, condensed chromatin structure with fragmented DNA started to appear inside cells but few were stained by PI, which could be characterized as early-apoptosis [41], [42]. As incubation time increased from 12 to 24 h, defects occurred in the cell membrane of apoptotic cells and allowed PI to enter the cytoplasm.

In Fig 5, the viability from fluorescence images and the corresponding number of internalized MNPs showed good linearity ($R^2 > 0.9999$) for both SKHep-1 and HeLa cells, which suggested nanotoxicity should have strong correlation with the number of intracellular MNPs. In Fig. 6, the MNP number obtained individually from dead/live cells were presented by box plot and cell-to-cell distinctions on MNPs uptake were appeared. Significantly differences between cellular MNP uptake in living and dead cells were observed after 12 h of incubation time ($p < 0.05$ for HepG2; $p < 0.01$ for SKHep-1, HeLa); as incubation time reached 24 h, the differences became more distinct for HeLa and SKHep-1 ($p < 0.001$) than HepG2 cell. Research suggested that there might be certain threshold for internalized NPs to exert effects on cell physiology [27]. Data of dead and live cells in the three incubation time (8, 12 and 24 h) were gathered to gain a possible range of MNP uptake that triggered cell death (shown in Fig. 6d). The comparison between the number of uptaken MNP in viable and non-viable cell were expressed as follow: SKHep-1 ((16 ± 4.08) vs. $(23 \pm 4.49) \times 10^6/\text{cell}$), HepG2 ((12.28 ± 3.63) vs. $(16.27 \pm 4.86) \times 10^6/\text{cell}$) and HeLa ((14.7 ± 3.71) vs. $(21.98 \pm 4.27) \times 10^6/\text{cell}$). Since the number of uptaken MNP is highly dependent on the endocytic activities, the number that obtained from the viable/non-viable cells of SKHep-1 and HeLa cell are much higher than that from HepG2 cell. Whereas, for the cells exhibited higher/lower activity or in phase between early-apoptosis to late apoptosis, the number of uptaken MNP would differ from the average and occurred as subpopulation in live/dead cell.

In our study, we proposed magnetophoresis combining fluorescence based cytotoxicity assay to evaluate the viability and the cellular MNPs uptake simultaneously at single cell level such that the influence of MNP number on cell viability of individual cells analyzed. Besides, using this method, endocytosis capacities of MNPs were analyzed individually and they exhibited cell-to-cell variations. So far, most of the previous studies estimated the

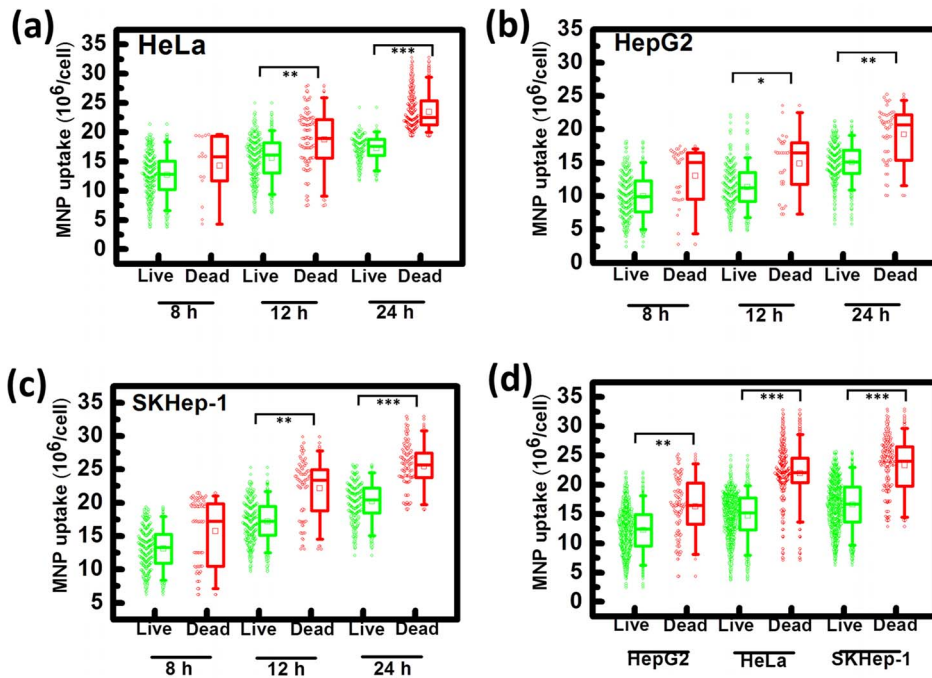


Figure 6. The variability of the number of intracellular MNPs obtained from live (green) and dead (red) cell. (a)–(c) are box plots of HeLa, HepG2 and SKHep-1, respectively. For each cell type, 500 cells that were treated with MNPs were analyzed at different co-culture times (8, 12, 24 h) to obtain the uptaken MNP number and viability of an individual cell. (d) is the data collection of all 1500 cells with different co-culture times (8, 12, 24 h) for each cell type. The dead/live cells were discriminated by the fluorescence images in the magnetophoresis experiment. The box represents the quartile distribution (25–75%) range. The median is indicated by a horizontal line and the mean is indicated by an open square inside the box. The whiskers mark 5–95% range of the distribution, and the outlier samples are indicated outside of this range. The scatter plots indicate the uptaken MNP number obtained from individual cell. Statistical significance between dead and live cells was determined using a student's t-test. The degree of significance was given as *: $p < 0.05$; **: $p < 0.01$; ***: $p < 0.001$. doi:10.1371/journal.pone.0096550.g006

concentration of iron oxide NPs by analyzing the constituent iron atoms or ions (Fe^{2+} , Fe^{3+}) dissociated from iron oxide NPs, whereas the magnetophoresis method used in the present study can directly derive the number of iron oxide NPs in their solid form.

Conclusions

In summary, magnetophoresis with fluorescence based cytotoxicity assay was proposed to evaluate the viability and MNPs loading simultaneously. By the method, endocytosis capacities of MNPs were analyzed individually to show cell-to-cell variations.

References

- Figuerola A, Di Corato R, Manna L, Pellegrino T (2010) From iron oxide nanoparticles towards advanced iron-based inorganic materials designed for biomedical applications. *Pharmacol Res* 62: 126–143.
- Jong WHD, Borm PJ (2008) Drug delivery and nanoparticles: applications and hazards. *Int J Nanomed* 2: 133–149.
- Ger TR, Huang HT, Huang CY, Liu WC, Lai JY, et al. (2014) Comparing the magnetic property of shell thickness controlled of Ag-Ni core-shell nanoparticles. *J Appl Phys* 115: 17B528 (3pp).
- Ger TR, Huang CY, Lai MF (2013) Cell Culture Arrangement Using Ferromagnetic Diamond-Shaped Thin Films. *MAG IEEE Trans* 49: 3453–3455.
- Hawkins MJ, Soon-Shiong P, Desai N (2008) Protein nanoparticles as drug carriers in clinical medicine. *Adv Drug Deliv Rev* 22: 876–85.
- Kovochich M, Marsden MD, Zack JA (2011) Activation of Latent HIV Using Drug-Loaded Nanoparticles. *PLoS ONE* 6: e18270.
- Ger TR, Huang HT, Huang CY, KS Hu, JY Lai, et al. (2014) Study of polyvinyl alcohol nanofibrous membrane by electrospinning as a magnetic nanoparticle delivery approach. *J Appl Phys* 115: 17B908 (3pp).
- Wang YX (2011) Superparamagnetic iron oxide based MRI contrast agents: Current status of clinical application. *Quant Imaging Med Surg* 1: 35–40.
- Na HB, Song IC, Hyeon T (2009) Inorganic Nanoparticles for MRI Contrast. *Agents Adv Mater* 21: 2133–2148.
- Ger TR, Huang HT, Chen WY, Lai MF (2013) Magnetically-controllable zigzag structures as cell microgripper. *Lab Chip* 13: 2364–2369.
- Ger TR, Huang HT, Huang CY, Lai MF (2013) Single cell detection using 3D magnetic rolled-up structures. *Lab Chip* 13: 4225–4230.
- Vallejo-Fernandez G, Whear O, Roca AG, Hussain S, Timmis J, et al. (2013) Mechanisms of hyperthermia in magnetic nanoparticles. *J Phys D: Appl Phys* 46: 312001 (6pp).
- Huang CY, Chen PJ, Ger TR, Hu KH, Peng YH, et al. (2014) Optimization of Magnetic Labeling Process for Intracellular Hyperthermia in Cervical Cancer Cells. *MAG IEEE Trans* 50: 1–4.
- Canton I, Battaglia G (2012) Endocytosis at the nanoscale. *Chem Soc Rev* 41: 2718–2739.
- Wang D, Bodovitz S (2010) Single cell analysis: the new frontier in 'Omics' *Trends Biotechnol.* 28: 281–290.
- Lu SS, Liu S, Zu QQ, Xu XQ, Yu J, et al. (2013) In vivo MR imaging of intraarterially delivered magnetically labeled mesenchymal stem cells in a canine stroke model. *PLoS One* 8: e54963.

The number of intracellular MNPs quantified by magnetophoresis was found to be strongly correlated with the viability and the differences between cellular MNP uptake in living and dead cells were distinctive. The method could be useful for future study of nanotoxicity induced by MNPs.

Author Contributions

Conceived and designed the experiments: CYH MFL ZHW. Performed the experiments: CYH TRG. Analyzed the data: CYH TRG. Contributed reagents/materials/analysis tools: CYH MFL. Wrote the paper: CYH ZHW.

17. Yocum TG, Wilson BL, Ashari P, Jordan KE, Frank AJ, et al. (2005) Effect of human stem cells labeled with ferumoxides-poly-L-lysine on hematologic and biochemical measurements in rats. *Radiology* 235: 547–552.
18. Riemer J, Hoepken HH, Czerwinska H, Robinson SR, Dringen R (2004) Colorimetric ferrozine-based assay for the quantitation of iron in cultured cells. *Anal Biochem* 331: 370–375.
19. Rad AM, Janic B, Iskander AS, Soltanian-Zadeh H, Arbab AS (2007) Measurement of quantity of iron in magnetically labeled cells: comparison among different UV/VIS spectrometric methods. *Biotechniques* 43: 627–628.
20. Lu AH, Salabas EL, Schueth F (2007) Magnetic Nanoparticles: Synthesis, Protection, Functionalization, and Application. *Angew Chem Int Ed* 46: 1222–1244.
21. Stroh A, Faber C, Neuberger T, Lorenz P, Sieland K, et al. (2005) Spatial smoothing of autocorrelations to control the degrees of freedom in fMRI analysis. *Neuroimage* 24: 635–641.
22. Wilhelm C, Gazeau F, Bacri JC (2002) Magnetophoresis and ferromagnetic resonance of magnetically labeled cells. *Eur Biophys J* 31: 118–125.
23. Jing Y, Mal N, Williams PS, Mayorga M, Penn MS, et al. (2008) Quantitative intracellular magnetic nanoparticle uptake measured by live cell magnetophoresis. *FASEB J* 22: 4239–4247.
24. Pisanic TR, Jin S, Shubayev VI (2009) Iron Oxide Magnetic Nanoparticle Nanotoxicity In: Sahu SC, Casciano DA, editors. *Incidence and Mechanisms, in Nanotoxicity* Chichester: John Wiley & Sons, Ltd, pp. 298–425.
25. Pisanic TR 2nd, Blackwell JD, Shubayev VI, Fiñones RR, Jin S (2007) Nanotoxicity of iron oxide nanoparticle internalization in growing neurons. *Biomaterials*. 28: 2572–2581.
26. Stroh A, Zimmer C, Gutzeit C, Jakstadt M, Marschinke F, et al. (2005) Iron oxide particles for molecular magnetic resonance imaging cause transient oxidative stress in rat macrophages. *Free Radical Biol Med* 36: 969–984.
27. Soenen SJ, Nuytten N, De Meyer SF, De Smedt SC, De Cuyper M (2010) High intracellular iron oxide nanoparticle concentrations affect cellular cytoskeleton and focal adhesion kinase-mediated signaling. *Small* 9: 832–842.
28. Soenen SJ, Rivera-Gil P, Montenegro J-M, Parak WJ, Smedt SCD, et al. (2011) Cellular toxicity of inorganic nanoparticles: common aspects and guidelines for improved nanotoxicity evaluation. *Nano Today* 6: 446–465.
29. Heffelfinger SC, Hawkins HH, Barrish J, Taylor L, Darlington GJ (1992) SK HEP-1: A human cell line of endothelial origin. *In Vitro Cell Dev Biol Anim* 28: 136–142.
30. Roe AL, Snawder JE, Benson RW, Roberts DW, Casciano DA (1993) HepG2 cells: an in vitro model for P450-dependent metabolism of acetaminophen. *Biochem Biophys Res Commun* 190: 15–19.
31. Rahbari R, Sheahan T, Modes V, Collier P, Macfarlane C, et al. (2009) A novel L1 retrotransposon marker for HeLa cell line identification. *BioTechniques* 46: 277–284.
32. Smirnov P (2009) Cellular magnetic resonance imaging using superparamagnetic anionic iron oxide nanoparticles: applications to in vivo trafficking of lymphocytes and cell-based anticancer therapy. *Methods Mol Biol* 512: 333–53.
33. Wilhelm C, Gazeau F (2008) Universal cell labelling with anionic magnetic nanoparticles. *Biomaterials* 29: 3161–3174.
34. Ger TR, Huang CY, Chiang CW, Fu PW, Hu KS, et al. (2013) Cell Patterning Using Magnetic Concentric Rectangular Thin Films for Biochip Application. *MAG IEEE Trans* 49: 3496–3499.
35. Strehel A, Harr T, Bachmann F, Wernli M, Erb P (2001) Green fluorescent protein as a novel tool to measure apoptosis and necrosis. *Cytometry* 43: 126–133.
36. Lamm GM, Steinlein P, Cotten M, Christofori G (1997) A rapid, quantitative and inexpensive method for detecting apoptosis by flow cytometry in transiently transfected cells. *Nucleic Acids Res* 25: 4855–4857.
37. Cogger VC, Arias IM, Warren A, McMahon AC, Kiss DL, et al. (2008) The response of fenestrations, actin, and caveolin-1 to vascular endothelial growth factor in SK Hep1 cells. *Am J Physiol Gastrointest Liver Physiol* 295: G137–G145.
38. Sylvester PW (2011) Optimization of the tetrazolium dye (MTT) colorimetric assay for cellular growth and viability. *Methods Mol Biol* 716: 157–168.
39. Berridge MV, Tan AS (1993) Characterization of the cellular reduction of 3-(4,5-dimethylthiazol-2-yl)-2,5-diphenyltetrazolium bromide (MTT): subcellular localization, substrate dependence, and involvement of mitochondrial electron transport in MTT reduction. *Archives Biochem Biophys* 303: 474–482.
40. Orrenius S, Nicotera P, Zhivotovsky B (2011) Cell Death Mechanisms and Their Implications in Toxicology. *Toxicol Sci* 19: 3–19.
41. Bredesen DE (1995) Neural apoptosis. *Ann Neurol* 38: 839–851.
42. Coleman ML, Sahai EA, Yeo M, Bosch M, Dewar A, et al. (2001) Membrane blebbing during apoptosis results from caspase-mediated activation of ROCK 1. *Nat Cell Biol* 3: 339–345.